DALTON
FULL PAPER

Chemical size effect on the magnetic and electrical properties of colossal magnetoresistance $La_{1.2}(Sr_{1.8-x}Ca_x)Mn_2O_7$ materials

Ru-Shi Liu,*[a] Chih-Hung Shen,[a] Jauyn Grace Lin,[b] Chao-Yuan Huang,[c] Jin-Ming Chen[d] and Ru-Gun Liu[d]

[a] *Department of Chemistry, National Taiwan University, Taipei, Taiwan, R.O.C. E-mail: rsliu@ccms.ntu.edu.tw*
[b] *Center for Condensed Matter Sciences, National Taiwan University, Taipei, Taiwan, R.O.C.*
[c] *Center for Condensed Matter Sciences and Department of Physics, National Taiwan University, Taipei, Taiwan, R.O.C.*
[d] *Synchrotron Radiation Research Center (SRRC), Hsinchu, Taiwan, R.O.C.*

Received 14th October 1998, Accepted 14th December 1998

Chemical size effects on the magnetic and electrical properties of the colossal magnetoresistance $La_{1.2}(Sr_{1.8-x}Ca_x)Mn_2O_7$ materials have been investigated. Based on the chemical shifts of the first unoccupied excited states in the core-level X-ray absorption spectrum correlated to the charge, the valence of Mn has been determined to be 3.43 ± 0.05 for all x in $La_{1.2}(Sr_{1.8-x}Ca_x)Mn_2O_7$. The magnetoresistance ratio $[\rho(0)/\rho(H)]$ can be efficiently increased from ≈192% (135 K, 1.5 T) for $x = 0$ to 208% (102 K, 1.5 T) for $x = 0.4$. On further increase in the concentration of Ca ($x = 0.6$ and 0.8) the samples only show a spin-glass behavior.

Introduction

Recently, Moritomo *et al.*[1] reported that a single crystal $La_{1.2}Sr_{1.8}Mn_2O_7$, the $n = 2$ member of the Ruddlesden–Popper series $(La,Sr)_{n+1}Mn_nO_{3n+1}$, is a ferromagnetic metal below T_C (Curie temperature) 130 K and a paramagnetic insulator above this temperature. They attribute the coupled electronic and magnetic transitions at T_C to a double exchange coupling in Mn^{3+}–O–Mn^{4+} linkages. Application of a magnetic field to this layered compound gives rise to an enhanced colossal magnetoresistance (CMR) ratio $[\rho(0)/\rho(H)] \approx 20\,000\%$ (≈130 K, $H = 7$ T). Moreover, this material may also be important due to its pronounced CMR at low field, ≈200% at ≈130 K in 0.3 T.

In the $(La,Sr)_{n+1}Mn_nO_{3n+1}$ system the dimensionality can vary depending on the number of perovskite layers controlled by the arrangement of octahedral MnO_6. The $n = 1$ member has a two-dimensional K_2NiF_4-type structure while $n = 2$ ($Sr_3Ti_2O_7$-type) and 3 ($Sr_4Ti_3O_{10}$-type) members would have a dimensionality between 2 and 3. The three-dimensional $(La,Sr)MnO_3$ containing an infinite number of perovskite layers is the $n = \infty$ member. Up to now the single-sheet ($n = 1$) compound has been examined and found to be a non-metallic antiferromagnet.[2,3] However, the double-sheet $(La,Sr)_3Mn_2O_7$ is a conducting ferromagnet with a CMR ratio higher than those of $n = 3$ and $n = \infty$.[1,4,5] This implies that a lower dimensionality is more favorable for CMR.

In comparison to the three-dimensional perovskites ($n = \infty$), the effect of band narrowing due to reduced dimensionality and novel arrangements of spins that are possible in the $n = 2$ series serve to make the $La_{1.2}Sr_{1.8}Mn_2O_7$ ($n = 2$) system an interesting subject of study. Recently Mitchell *et al.*[6] reported that, unlike the three-dimensional system, the Jahn–Teller distortion of the MnO_6 octahedra in this quasi-two-dimensional $La_{1.2}Sr_{1.8}Mn_2O_7$ ($n = 2$) material increases as charge is delocalized below T_C. Moreover, as the external (hydrostatic) pressure is applied the T_C increases linearly in $La_{1.2}Sr_{1.8}Mn_2O_7$ which reflects the competition between double and superexchange resulting from two-dimensional Mn–O–Mn networks along the c axis and can be interpreted in terms of the exchange striction model.[7] Moreover, the defects (*i.e.* intergrowth with other Ruddlesden–Popper phases) as observed by high-resolution transmission electron microscopy (HRTEM) in $n = 2$ materials are likely to have some effects on the magnetotransport properties.[8,9]

Here, we demonstrate the synthesis and chemical size effect (by the substitution of isovalent smaller Ca^{2+} ions into the bigger Sr^{2+} sites; corresponding to the internal pressure) on the magnetic and electrical properties of the CMR $La_{1.2}(Sr_{1.8-x}Ca_x)Mn_2O_7$ materials. The results may help us to understand the origin of the CMR effect in these quasi-two-dimensional manganites.

Experimental

The samples of $La_{1.2}(Sr_{1.8-x}Ca_x)Mn_2O_7$ with $x = 0$–0.8 were prepared by mixing high purity powders of La_2O_3, $SrCO_3$, $CaCO_3$ and MnO_2. The mixtures were calcined in air at 1200 °C for 24 h, 1400 °C for 24 h and 1500 °C for 24 h with intermediate grinding after each heating step. The resulting mixtures were ground and pressed into pellets then sintered at 1500 °C for 24 h in air.

X-Ray powder diffraction measurements were carried out with a SCINTAG (X1) diffractometer (Cu-Kα radiation). Data for the Rietveld refinement were collected in the 2θ range 20–120° with a step size of 0.02° and a count time of 10 s per step. The program GSAS[10] was used for the Rietveld refinement in order to obtain information on the crystal structure of $La_{1.2}(Sr_{1.8-x}Ca_x)Mn_2O_7$.

The valence of Mn was determined by the X-ray absorption technique. Experiments were carried out at the Synchrotron Radiation Research Center (SRRC) in Taiwan with an electron beam energy of 1.5 GeV and a maximum stored current of 240 mA. Horizontal and vertical focusing spherical mirrors coated with gold were used to collect 10 mrad of radiation. The synchrotron radiation was then monochromatized by a 6 m high-energy spherical grating monochromator (HSGM) which covers the photon energy range of 150–1200 eV. The monochromatized beam was refocused by a bent toroidal glidcop mirror onto the sample position. The focused beam size

Table 1 Crystallographic data for $La_{1.2}(Sr_{1.8-x}Ca_x)Mn_2O_7$ ($x = 0.2$)

Atom	x	y	z	Fraction	10^2U_{iso}/Å^2	Interatomic distances/Å	
La(P)	0	0	0.5	0.525	1.98(7)	(La,Sr,Ca)(P)–O(1) × 4	2.7374(1)
Sr(P)	0	0	0.5	0.422	1.98(7)	(La,Sr,Ca)(P)–O(2) × 8	2.741(7)
Ca(P)	0	0	0.5	0.053	1.98(7)	(La,Sr,Ca)(R)–O(2) × 4	2.608(7)
La(R)	0	0	0.31632(9)	0.3375	2.60(6)	(La,Sr,Ca)(R)–O(3) × 1	2.44(2)
Sr(R)	0	0	0.31632(9)	0.5885	2.60(6)	(La,Sr,Ca)(R)–O(3) × 4	2.746(1)
Ca(R)	0	0	0.31632(9)	0.074	2.60(6)	Mn–O(1) × 1	1.944(4)
Mn	0	0	0.0968(2)	1	1.45(7)	Mn–O(2) × 4	1.93562(7)
O(1)	0	0	0	1	4.0(8)	Mn–O(3) × 1	1.97(2)
O(2)	0	0.5	0.0966(5)	1	4.0(8)		
O(3)	0	0	0.8053(8)	1	4.0(8)		

Space group *I*4/*mmm*, $a = b = 3.8712(1)$, $c = 20.0785(8)$ Å, $V = 300.91(2)$ Å^3, $R_p = 10.85\%$, $R_{wp} = 14.38\%$, $\chi^2 = 3.024$. (P) = Perovskite site; (R) = rock-salt site.

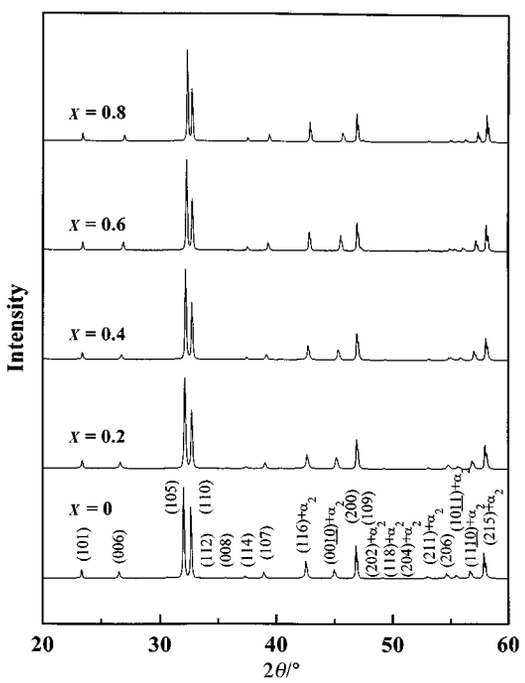

Fig. 1 Powder XRD spectra of the $La_{1.2}(Sr_{1.8-x}Ca_x)Mn_2O_7$ ($x = 0$–0.8) samples (α_2 represents non-monochromatic radiation).

at the sample position is about 1 × 1 mm. The second-order harmonic light from the 6 m HSGM is about 1–6% in the whole scanning range 110–500 eV covered by a 400 lines mm^{-1} grating. For the present manganese 2p-edge X-ray absorption measurements a 1200 lines mm^{-1} grating was used. The high-order diffraction contribution is expected to be very small for this higher ruled density grating since higher energies are covered. The X-ray absorption spectra were recorded by measuring the sample current. The incident photon flux (I_o) was monitored simultaneously by a nickel mesh located after the exit slit of the monochromator. All the measurements were normalized to I_o. The manganese 2p-edge X-ray absorption spectra were recorded from 635 to 665 eV with a scan step of 0.1 eV. Two cycles of runs were performed for each sample. The reproducibility of the absorption spectra of the same sample in different experimental runs was found to be extremely good. The photon energies were calibrated within an accuracy of 0.1 eV *via* the known oxygen K-edge absorption peaks of CuO. The energy resolution of the monochromator was set to ≈0.25 eV at an incident photon energy of 640 eV. All the measurements were performed at room temperature.

Magnetization data were taken from a superconducting quantum interference device (SQUID) magnetometer (Quantum Design) *via* zero-field cooling at a field of 0.1 T. Bar-shape samples were cut from the sintered pellets to be used for the standard four-probe resistivity measurements.

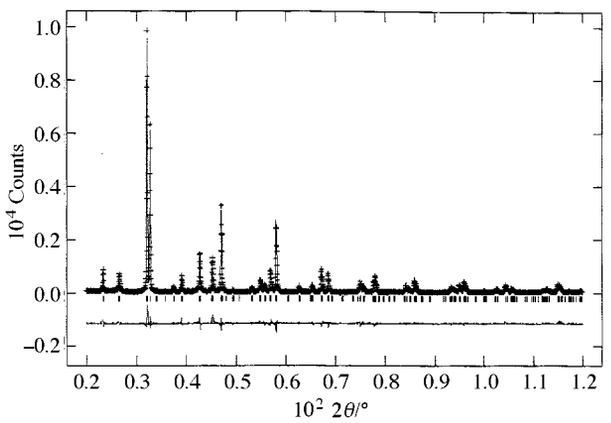

Fig. 2 Observed, calculated and difference X-ray powder diffraction patterns for $La_{1.2}(Sr_{1.8-x}Ca_x)Mn_2O_7$ ($x = 0.2$) at 300 K. Reflection positions are marked for the phase.

Results and discussion

The powder XRD spectra of the $La_{1.2}(Sr_{1.8-x}Ca_x)Mn_2O_7$ ($x =$ 0–0.8) samples are shown in Fig. 1. The series samples are single phase. All the peaks in each pattern can be indexed with a tetragonal cell and space group *I*4/*mmm*. Here, we present a typical example of crystallographic data in Table 1 and the observed and calculated diffraction profiles in Fig. 2 for the $La_{1.2}(Sr_{1.8-x}Ca_x)Mn_2O_7$ ($x = 0.2$) sample. Battle *et al.*[11,12] have demonstrated by the neutron power diffraction technique that $Nd_{1+x}Sr_{2-x}Mn_2O_7$ samples display phase separation due to the coexistence of two $n = 2$ phases with very similar unit-cell volumes. The two phases appear to differ only in the distribution of the Sr^{2+} and Nd^{3+} cations over the two available (La,Sr,Ca) cation sites. However, due to the instrumental limits, it is very difficult to use the X-ray powder diffraction data to do the occupancy refinements for such complex cation substitutions.† Here, we assume that the Ca^{2+} ions substituted into the Sr^{2+} sites follow the distribution as shown by the model in ref. 13. We therefore kept the occupancies constant for the (La,Sr,Ca) sites in our data refinements. In Fig. 3 an ideal crystal structure of $(La,Sr,Ca)_3Mn_2O_7$ which consists of double perovskite layers, each layer made up of a two-dimensional network of MnO_6 octahedra, is shown. Alternate perovskite bilayers along the *c* axis are misarranged with respect to each other. The lattice constants (*a* and *c*) decrease as the calcium (x) content increases (as shown in Fig. 4). Moreover, a decrease in cell volume with increasing x was also found (Fig. 5).

† The quality of the Rietveld refinements presented here indicates that the problem of coexistence of two similar Ruddlesden–Popper phases due to different cation distributions over the available A cation sites, first described for $Nd_{1+x}Sr_{2-x}Mn_2O_7$, may well be the case here.

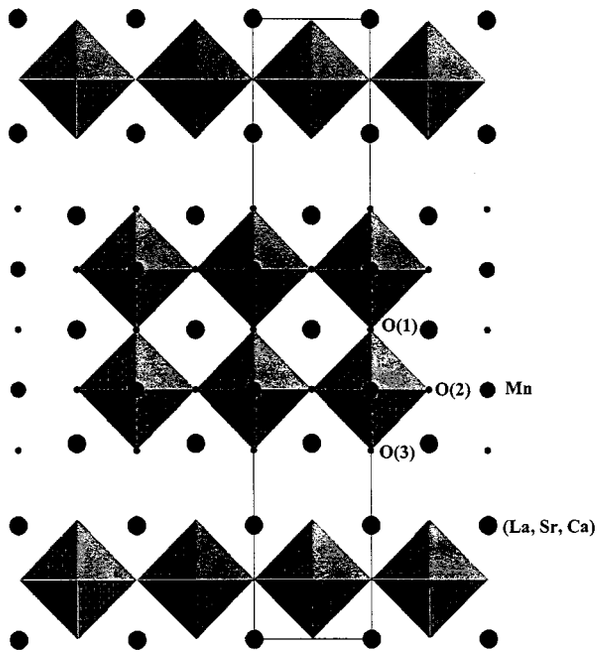

Fig. 3 The crystal structure of $(La,Sr,Ca)_3Mn_2O_7$ projected along the c axis. The unit cell is shown with a solid line. The MnO_6 octahedra are shaded.

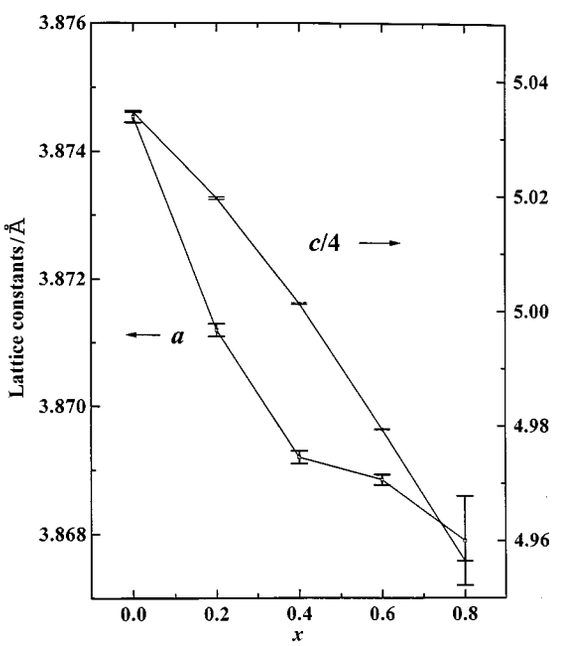

Fig. 4 Lattice constants a and c as a function of x in $La_{1.2}(Sr_{1.8-x}Ca_x)Mn_2O_7$ ($x = 0$–0.8).

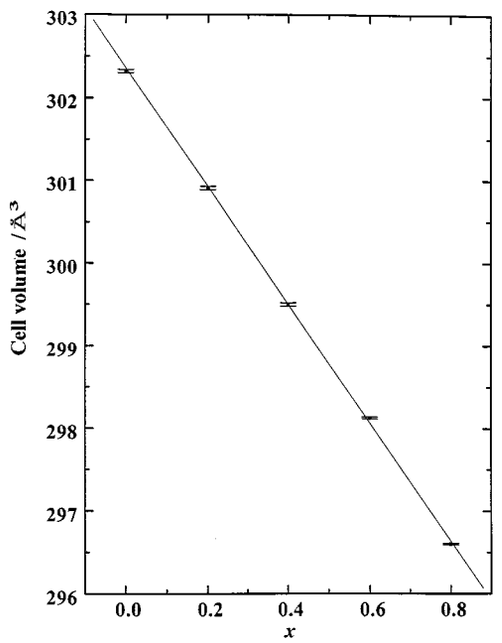

Fig. 5 Cell volume as a function of x in $La_{1.2}(Sr_{1.8-x}Ca_x)Mn_2O_7$ ($x = 0$–0.8).

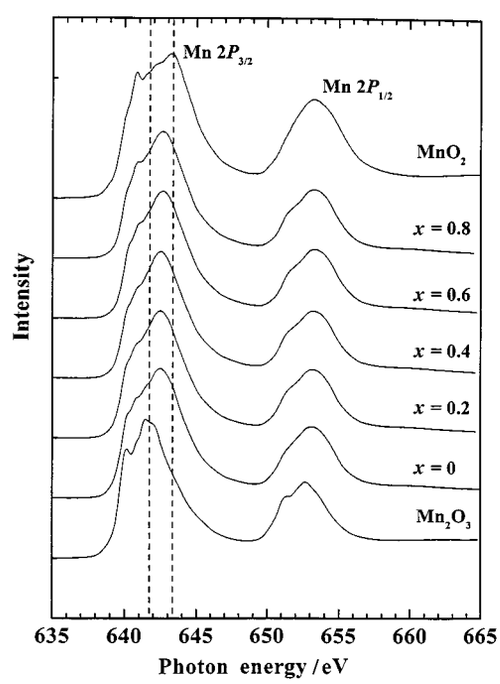

Fig. 6 Manganese 2p-edge X-ray absorption near edge structure spectra of MnO_2 (Mn^{4+}), Mn_2O_3 (Mn^{3+}) and $La_{1.2}(Sr_{1.8-x}Ca_x)Mn_2O_7$ ($x = 0$–0.8).

These are simply due to a manifestation of the smaller size of the substituting Ca^{2+} ion [1.18 Å for CN (co-ordination number) = 9] as compared to the bigger Sr^{2+} ions (1.31 Å for CN = 9).[14]

The manganese 2p-edge X-ray absorption near edge structure (XANES) spectra of $La_{1.2}(Sr_{1.8-x}Ca_x)Mn_2O_7$ are shown in Fig. 6. For comparison, the spectra of MnO_2 (Mn^{4+}) and Mn_2O_3 (Mn^{3+}) are also plotted. The spectra show two broad multiplet structures separated by spin–orbit splitting (Mn $2p_{3/2}$ and $2p_{1/2}$). The chemical shift is caused by changes in the electrostatic energy at the Mn driven by the variation of the ionic valence in the compounds. It is well established that the effective ionic valence can be measured from the chemical shift of the core-level X-ray photoemission.[15] We, therefore, adopted the same scheme to obtain the manganese valence of around 3.43 ± 0.05 across the series $La_{1.2}(Sr_{1.8-x}Ca_x)Mn_2O_7$. All the values of the valence are consistent with those deduced from the nominal composition $La_{1.2}(Sr_{1.8-x}Ca_x)Mn_2O_7$. Therefore, a mixture of Mn^{3+} and Mn^{4+} is present in this system.

In Fig. 7 we show the temperature dependence of the magnetization at a magnetic field of 0.1 T for the series $La_{1.2}(Sr_{1.8-x}Ca_x)Mn_2O_7$. In the temperature range 100–130 K it indicates a sharp paramagnetic to ferromagnetic transition in $x = 0$, 0.2 and 0.4 samples. A decrease in T_C's from 135 K for $x = 0$ to 102 K for $x = 0.4$ was found (as shown in the inset of Fig. 7). This suggests that the small Ca^{2+} ions substituted into the bigger Sr^{2+} ionic sites will increase the internal chemical pressure within the compound which may lead to a decrease in T_C. The results are somewhat different as compared to the hydrostatic effect which results in an increase in T_C with increasing external pressure. Moreover, a small but real kink

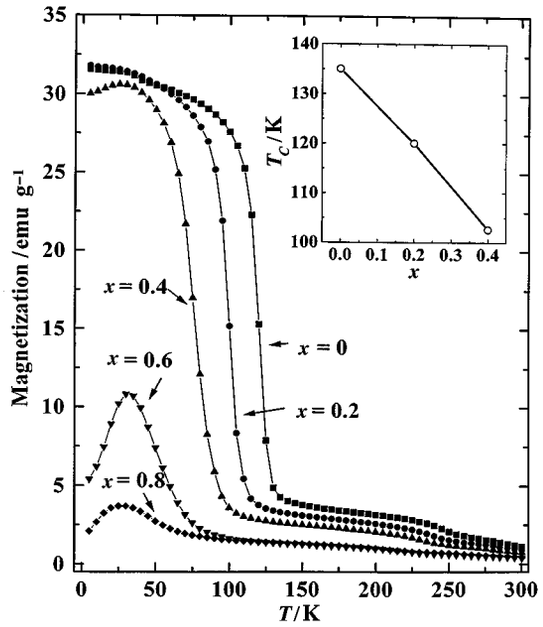

Fig. 7 Temperature dependence of the magnetization at a magnetic field of 0.1 T for the series $La_{1.2}(Sr_{1.8-x}Ca_x)Mn_2O_7$ (x = 0–0.8).

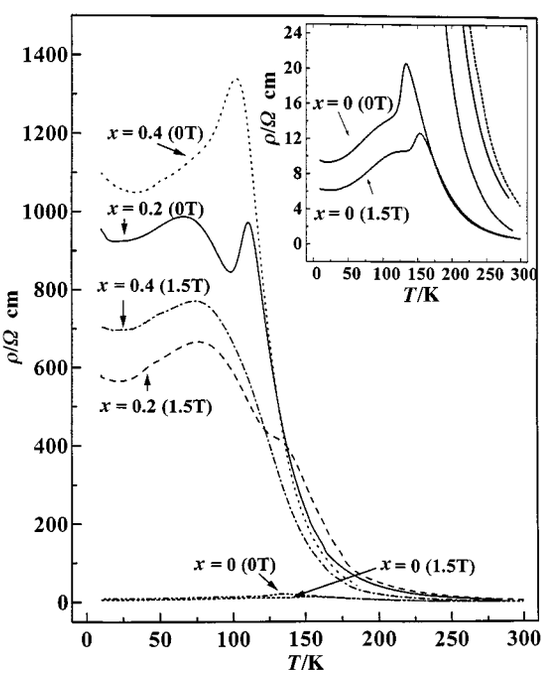

Fig. 8 Temperature dependence of the resistivity of the $La_{1.2}(Sr_{1.8-x}Ca_x)Mn_2O_7$ (x = 0–0.8) compounds in the absence and presence of a 1.5 T magnetic field.

appeared at 250 K in the M *vs.* T curve for the x = 0–0.4 samples which may be due to the two-dimensional spin correlation.[1] When $x > 0.4$ a cusp structure at ≈30 K was exhibited for the x = 0.6 and 0.8 samples which may correspond to spin-glass behavior due to competition between ferro- and antiferro-magnetic interactions.

In Fig. 8 we show the temperature dependence of the resistivity of the $La_{1.2}(Sr_{1.8-x}Ca_x)Mn_2O_7$ compounds in the absence and presence of a 1.5 T magnetic field. All the samples show a peak corresponding to a transition from the semiconducting to the metallic state when the temperature is decreased. The transition temperature (T_m) at zero field decreases from 135 K for x = 0 to 102 K (as shown in Fig. 9) for x = 0.4 as Sr^{2+} is replaced by Ca^{2+} in $La_{1.2}(Sr_{1.8-x}Ca_x)Mn_2O_7$, consistent with the T_C as measured by the magnetic method (as shown in Fig. 7).

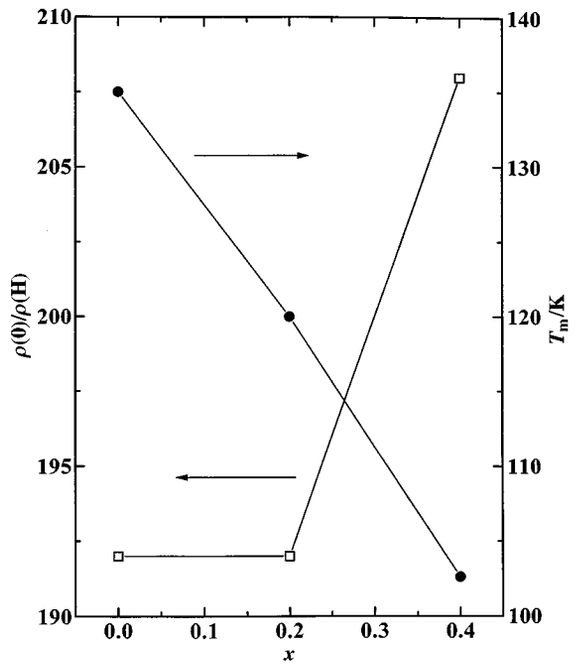

Fig. 9 Magnetoresistance ratio [$\rho(0)/\rho(H)$] and transition temperature (T_m) at zero field as a function of x in $La_{1.2}(Sr_{1.8-x}Ca_x)Mn_2O_7$ (x = 0–0.8).

The magnetoresistance [$\rho(0)/\rho(H)$] ratio is increased from ≈192% (135 K, 1.5 T) for x = 0 to 208% (102 K, 1.5 T) for x = 0.4 in $La_{1.2}(Sr_{1.8-x}Ca_x)Mn_2O_7$ (as shown in Fig. 9). This means that the highest magnetoresistance ratio can be obtained by tuning the ionic size between Ca^{2+} and Sr^{2+} in $La_{1.2}(Sr_{1.8-x}Ca_x)Mn_2O_7$. Also of note is the broad transition at temperatures lower than 100 K in the resistivity curves for all the samples as shown in Fig. 8. This phenomenon is similar to that of the $LaSr_2Mn_2O_7$ sample and was attributed to the coexistence of ferromagnetic and antiferromagnetic correlation.[16]

Argyriou *et al.*[7] have pointed out that at low temperatures the spins of neighboring manganese atoms are ordered ferromagnetically within each MnO_2 plane but exhibit a non-zero cant angle for the coupling between planes in the $La_{1.2}Sr_{1.8}Mn_2O_7$ compound. Such canted magnetic order is due to the competition between the interactions of the Mn atoms with the $t_{2g}e_g$ electronic configuration. The t_{2g} electrons in the half filled band are localized and participate in antiferromagnetic bonding between the MnO_2 planes. The e_g electrons are hybridized with the oxygen 2p states creating chemical Mn–O–Mn bonds within the MnO_2 planes. Chemical substitution of La^{3+} by Sr^{2+} in $La_{1.2}Sr_{1.8}Mn_2O_7$ introduces Mn^{4+} ions into the lattice and holes into the e_g band. This double exchange e^1–p_σ–e^0 interaction between the Mn^{3+} and Mn^{4+} ions favors a ferromagnetic spin coupling. Therefore, detailed and precise crystal structure data including bond angles and distances as determined by neutron diffraction across the $La_{1.2}(Sr_{1.8-x}Ca_x)Mn_2O_7$ series are needed to investigate the mechanism of the magnetic and electrical properties.

In conclusion, this study has demonstrated that the size of the interpolated cation obtained by tuning the concentration between Ca^{2+} and Sr^{2+} plays a role in controlling the magneto-transport properties of the colossal magnetoresistance $La_{1.2}(Sr_{1.8-x}Ca_x)Mn_2O_7$ materials.

Acknowledgements

This research is financially supported by the National Science Council of the Republic of China under grant numbers NSC 87-2112-M-002-032 and NSC 88-2113-M-002-029.

References

1 Y. Moritomo, A. Asamitsu, H. Kuwahara and Y. Tokura, *Nature* (*London*), 1996, **380**, 141.
2 C. N. R. Rao, P. Ganguly, K. K. Sing and R. A. Mohan Ram, *J. Solid State Chem.*, 1988, **72**, 14.
3 Y. Moritomo, Y. Tomioka, A. Asamitsu, Y. Tokura and Y. Matsui, *Phys. Rev. B*, 1995, **51**, 3279.
4 R. Mahesh, R. Mahendiran, A. K. Raychaudhuri and C. N. R. Rao, *J. Solid State Chem.*, 1996, **122**, 448.
5 R. Seshadri, C. Martin, M. Hervieu, B. Raveau and C. N. R. Rao, *Chem. Mater.*, 1997, **9**, 270.
6 J. F. Mitchell, D. N. Argyriou, J. D. Jorgensen, D. G. Hinks, C. D. Potter and S. D. Bader, *Phys. Rev. B*, 1997, **55**, 63.
7 D. N. Argyriou, J. F. Mitchell, J. B. Goodenough, O. Chmaissem, S. Short and J. D. Jorgensen, *Phys. Rev. Lett.*, 1997, **78**, 1568.
8 R. Seshadri, M. Hervieu, C. Martin, A. Maignan, B. Domenges and B. Raveau, *Chem. Lett.*, 1997, **9**, 1778.
9 J. Sloan, P. D. Battle, M. A. Green, M. J. Rosseinsky and J. F. Vente, *J. Solid State Chem.*, 1998, **138**, 135.
10 A. C. Larson and R. B. Von Dreele, GSAS, Generalized Structure Analysis System, Los Alamos National Laboratory, Los Alamos, NM, 1994.
11 P. D. Battle, M. A. Green, N. S. Laskey, J. E. Millburn, P. G. Radaelli, M. J. Rosseinsky, S. P. Sullivan and J. F. Vente, *Phys. Rev. B*, 1996, **54**, 15967.
12 P. D. Battle, J. A. Hepburn, J. E. Millburn, P. G. Radaelli, M. J. Rosseinsky, L. E. Spring and J. F. Vente, *Chem. Mater.*, 1997, **9**, 3215.
13 R. Seshadri, C. Martin, A. Maignan, M. Hervieu, B. Raveau and C. N. R. Rao, *J. Mater. Chem.*, 1996, **6**, 1585.
14 R. D. Shannon, *Acta Crystallogr.*, *Sect. A*, 1976, **32**, 751.
15 A. T. Carlson, *Photoelectron and Auger Spectroscopy*, Plenum, New York, 1975.
16 R. Seshadri, A. Maignan, M. Hervieu, N. Nguyen and B. Raveau, *Solid State Commun.*, 1997, **101**, 453.

Paper 8/07978A